Lattice Design for a Very High Brightness X-Ray Storage Ring

Ken Soong
Physics, Cornell University, Ithaca, NY, 14853
(Dated: August 9, 2007)

The single most important quantity characterizing x-ray beams is their brilliance (also known as spectral brightness). In order to produce high brilliance it is necessary for the electron beam to have a small emittance. The emittance of a beam is in turn determined by the sequence of magnets through which the beam travels. When referring to a storage ring, this sequence of magnets (dipoles and quadrupoles) is known as the magnet lattice. In this paper a modification to the design of the dipole bending magnet is given, as well as a refined magnet lattice design. Together, these two modifications will allow the existing Cornell Electron Storage Ring (CESR) to be upgraded (at a low cost) to become the brightest source of hard x-rays in the United States.

I. INTRODUCTION

The existing Cornell Electron Storage Ring (CESR) accelerator is an electron-positron colliding beam facility used primarily for research in high-energy physics. When electrons or positrons travel around the storage ring, x-rays are naturally emitted as a byproduct. These x-rays have a significantly higher brilliance and are better collimated than those available from compact laboratory x-ray sources, such as rotating anode x-ray tubes, and thus serve as a valuable research tool. The brilliance of an x-ray beam, or its spectral brightness, is a measure of the number of photons that can be delivered to samples. More rigorously, it is defined as a number of photons per second per unit area and solid angle per 0.1% bandwidth. In order to produce high brilliance, it is essential for the primary (electron) beam to have a small emittance, which is the product of its width and its angular divergence at the location of the beam waist. For most applications, the brilliance of an x-ray beam is the single most important characteristic.

Talman in his report [1] presents a plan to convert the existing CESR facility into a dedicated high brilliance x-ray source, which would put the ring on the brilliance frontier. The design would use existing storage ring components, to the extent possible, and conserve the ring footprint of the Wilson tunnel. In this spirit, it is essential to find a way to modify the dipole bending magnets, a major constituent in the lattice, to be compliant with the new design. Furthermore, to preserve the ring footprint of the Wilson tunnel, the strength of the bending magnets as well the layout of the magnet lattice would have to be adjusted. However, to avoid increased emittance and reduce dispersion, it is also necessary to keep the magnet strengths as nearly unchanged as possible.

II. BENDING MAGNETS

The existing CESR operates with eighty-four bending magnets. These C-magnets have a constant magnetic field in the region between the magnetic poles and serve to constrain the electron beam to follow the footprint of Wilson tunnel, see Fig. 1. However, there is a tendency for the electrons to diverge and thus a need for the electrons to be restrained by

focusing elements. The uniform magnetic field of the bending magnets weakly focuses the particle beam in the horizontal direction, but does not have a focusing effect in the vertical direction. As such, any particle that is vertically displaced from the center of the beam will continue to diverge from the beam until it is lost (that is in the absence of so-called strong focusing, or quadrupoles). To overcome this problem, the bending magnets can be shaped so that the field develops a gradient along the vertical direction, namely $\frac{\partial B_x}{\partial y} \neq 0$. Thereafter, any electrons above the center of the beam, $y > 0$, will feel a force downwards and any electrons below the center, $y < 0$, will feel a force upwards. An additional benefit of the above mentioned weak focusing is its ability to redistribute the damping partition numbers, which lead to a further decrease in transverse beam emittance [5].

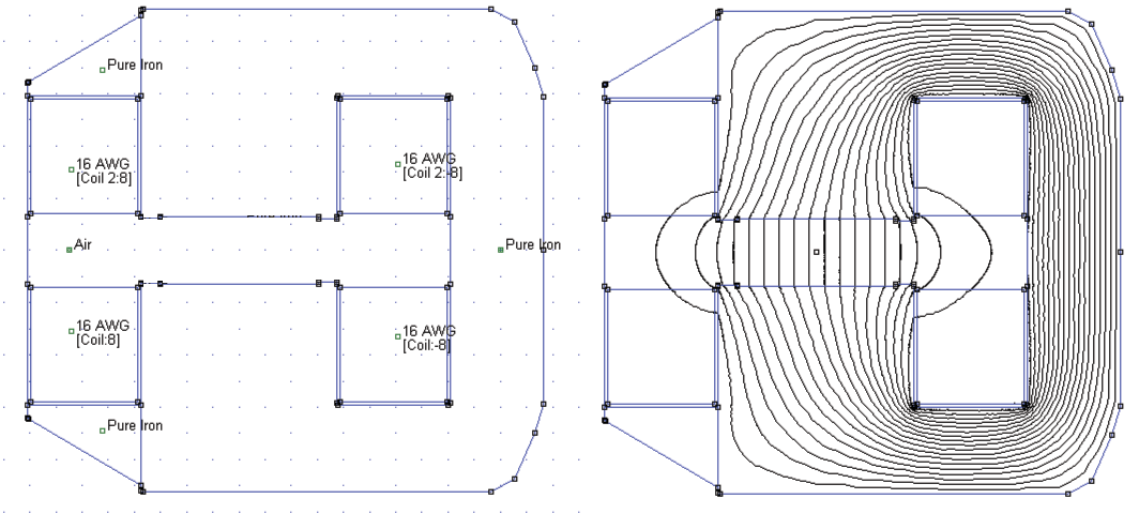

FIG. 1: A cross sectional view of the existing dipole bending magnet. The figure on the left shows the composition of the dipole magnet, while the figure on the right shows the magnetic field lines created by the magnet. The density of the field lines is proportional to the magnetic field strength. From the figure on the right, we can see that the region between the magnet poles have a constant density of field lines and thus a constant magnetic field strength. These figures were created using FEMM.

However, the solution to the problem is constricted by the condition $\frac{\partial B_y}{\partial x} = \frac{\partial B_x}{\partial y}$. This relationship limits the ability for the bending magnets to focus the beam, since any additional focusing in the vertical direction will reduce the focusing in the horizontal direction and vice versa, see Fig. 2. Because the brilliance of the resulting x-rays depends on the electron beam properties through the proportionality $B \propto \frac{I}{\epsilon_x \epsilon_y}$, it is possible to adjust the amount of focusing in each direction to maximize the overall brilliance [2]. This effect is most generally seen in equations as a term called the quadrupole coefficient,

$$K_1 = \frac{\partial B_y}{\partial x} \frac{1}{B\rho}. \tag{1}$$

The calculated optimal value of the quadrupole coefficient in [1] was found to be $K_1 = -0.07$ for the CESR lattice.

Due to the impracticality of re-machining the existing bending magnets, we agreed that designing an iron crown to be attached to the magnets would be the most feasible approach

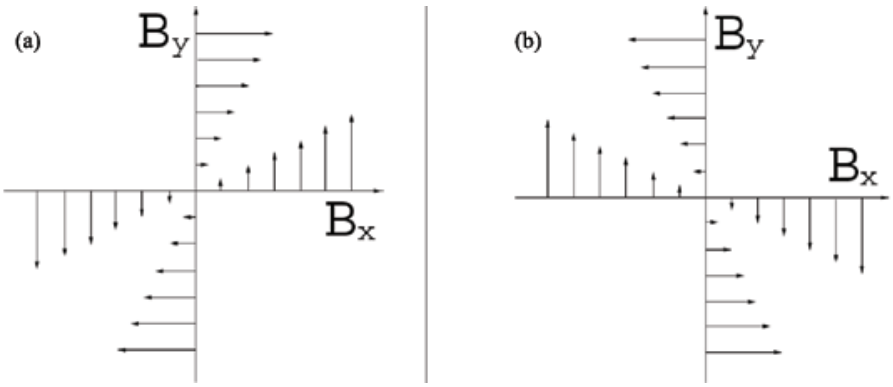

FIG. 2: A rendering of the expected magnetic field strength at the center of our modified magnets. Here two cases are given, one with a positive gradient and one with a negative gradient. In both case the strengths are constrained by $\frac{\partial B_y}{\partial x} = \frac{\partial B_x}{\partial y}$. These figures should be accurate up to the addition of a constant to B_x and/or B_y. By applying the right-hand rule to a hypothetical off-center particle, it can be seen that a focusing in one plane must lead to a defocusing in the other plane.

to modifying the field strength of the magnets. These crowns were designed using the program Finite Element Method Magnetics (FEMM), Version 4.0. FEMM is a computer-aided design program with the built-in capability of calculating the magnetic fields of a region. The program does so by solving the equation,

$$-\frac{1}{\mu}\nabla^2 A = J \tag{2}$$

which is derived directly from Maxwell's equations. Once the vector potential A is found, B and H can be deduced by differentiating A. Although the differential equation (2) looks relatively simple, it is typically very difficult to get closed-form solutions for all but the simplest geometries. To overcome this dilemma, FEMM utilizes the idea of finite element analysis, where the problem is broken down into a large number of regions, each with a simple geometry. Over these regions, the solution for the potential is approximated with a simple function, which, for small enough regions, will closely match the exact solution [3].

With no further restrictions, it is conceivable that we could design a crown that would produce a magnetic field to match any pattern we desire. However, the designing of the iron crown is complicated by considerations for the ease of production and the specifications of the vacuum chamber, which will be situated between the crowns, see Fig. 4. With considerations for the vacuum chamber, we restrict the crowns to have a height which is no greater than $\frac{1}{6}$ of the gap between the current magnet's poles. Further, we require that our gradient $\frac{\partial B_y}{\partial x}$ span at least a seven centimeter region along the x-axis at $y = 0$, termed the "good field region", as well as requiring a region of uniform field in which the vacuum pump chamber would reside. Fig. 3 shows our crown design, which match all of the constraints listed, while Fig. 5 shows the resulting gradient $\frac{\partial B_y}{\partial x}$ when the crowns are attached to the bending magnets. A linear regression of the resulting magnetic field produce the equation $B_y[\mathrm{T}] = 0.387273 - 1.1868x[\mathrm{m}]$ with an R^2 value of 0.9999. Here the good field region spans 10.45cm and is defined as all consecutive points which fall within 0.15% of the value predicted by the regression equation.

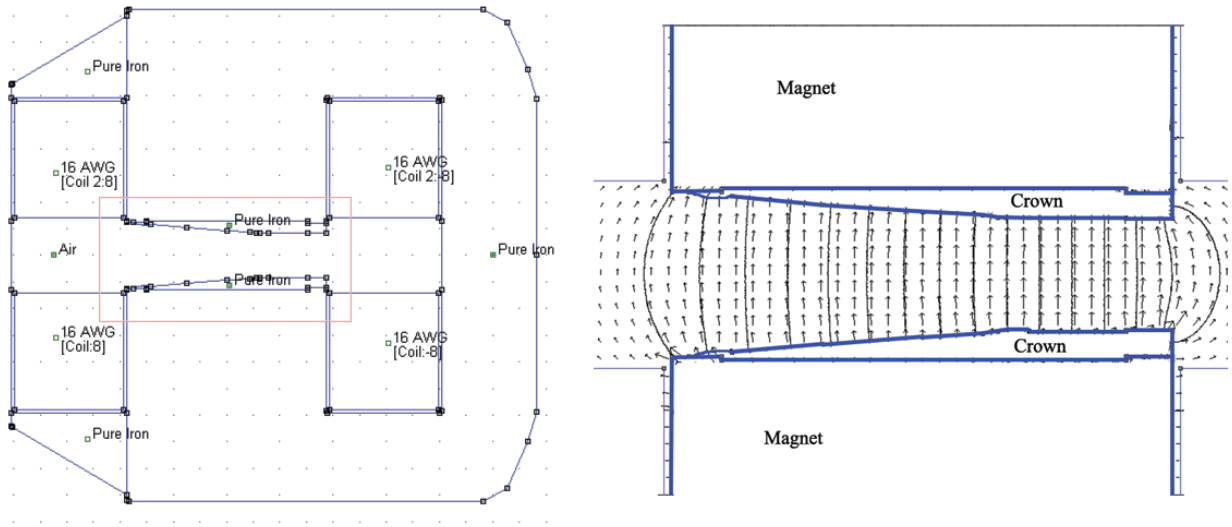

FIG. 3: A cross sectional view of the modified bending magnet. The figure on the left shows the composition of the modified bending magnet, while the figure on the right is a close up view of the magnetic field lines created by the magnet. The arrows in the figure indicate the strength and direction of the magnetic field. These figures were again created using FEMM.

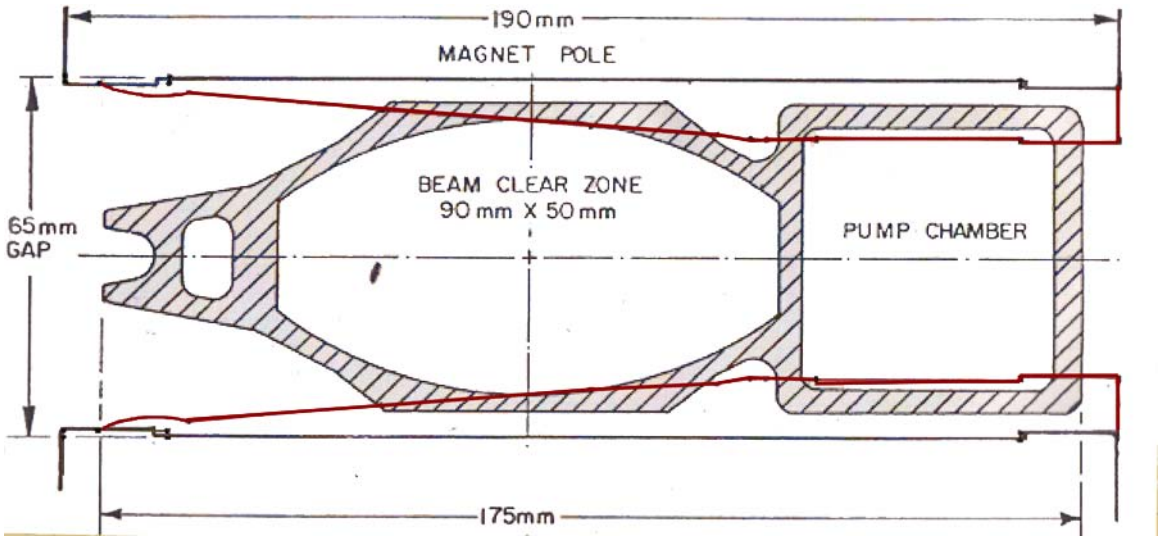

FIG. 4: A diagram of the current vacuum chamber with the proposed crowns superimposed. It is clear that the current vacuum chamber is too small to be used in conjunction with the iron crowns and will have to be redesigned. The sloped section of the crown will provide the necessary quadrupole effect in the beam clear zone, while the level section provides a uniform field for the pump chamber.

At near light speeds, where $\beta \approx 1$, and with electron energies $\varepsilon_e = 5.11[\text{GeV}]$, equation (1) for calculating the quadrupole coefficient can be written as $K_1 = 0.058669\frac{\partial B_y}{\partial x}$. Using the slope obtained from our crown design, $\frac{\partial B_y}{\partial x} = -1.1868$, we obtain a quadrupole coefficient value of $K_1 = -0.0696$.

To ensure that attaching the crowns were in fact feasible, we calculated the forces on

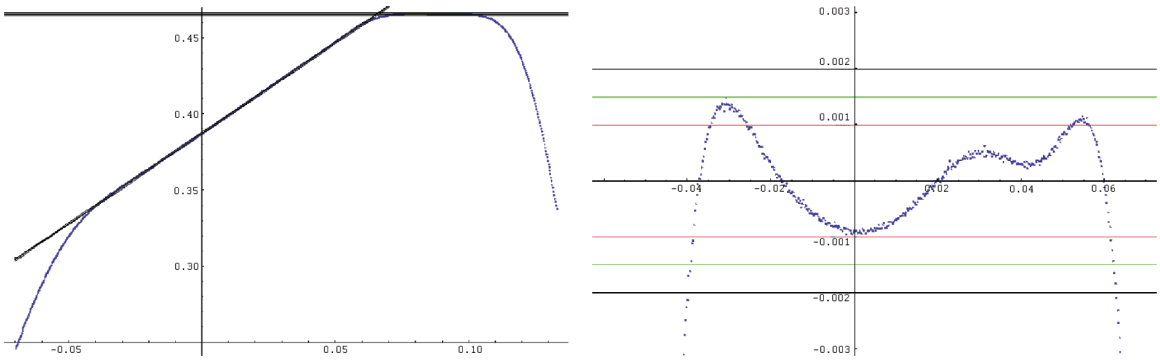

FIG. 5: The graph on the left is a plot of the field B_x along the line $y = 0$; linear regressions of both the good field region and uniform field zone are superimposed on this graph. The graph on the right contains a plot of the percentage of error for the regression of the good field region. The good field region for this design spans 10 cm, with errors of less than 0.2%.

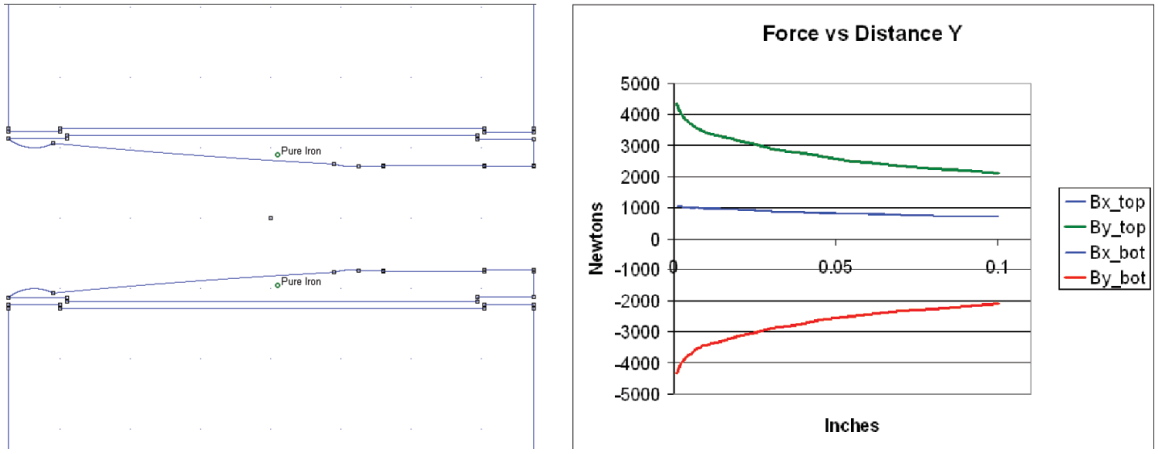

FIG. 6: The figure on the left shows a setup where the crowns were displaced a small amount from the ends of the magnet. This setup was used to calculate the forces on the crowns and the results are plotted on the right. A positive value of the force corresponds to the up or right direction, while a negative value corresponds to the down or left direction. The green line represents the force resulting from B_y on the upper crown, while the red line represents the force resulting from B_y on the lower crown. The blue line, on the other hand, represents the force resulting from B_x on both the upper and lower crown.

each crown. Using FEMM, we designed a system where the crowns were initially displaced a small distance from the ends of the magnet. We then applied the magnetic field and calculated the forces experienced by each crown, see Fig. 6. Had the crowns experienced a net force directed away from the ends of the magnets, then it would have been extremely impractical, if not impossible, to hold the crowns in place. Luckily, the crowns experienced a force directed towards their respective ends of the magnets, thus re-enforcing the adhesion between the crown and the magnet. For this reason, it is likely that once the magnets are turned on, the crowns would no longer strain their fastenings.

To determine the emittance of a beam, we used a program known as Methodical Accelerator Design (MAD), version 8. MAD is a tool for charged particle optics in accelerators

and beam lines. The MAD program can, among other features, calculate various linear lattice parameters , match linear lattices, and do survey calculations [4]. We began with a MAD lattice file designed in the original plan [1]. This design consisted of six sectors containing magnet lattices composed of bending magnets, quadrupoles, sextupoles and straight sections. Long straight sections divided each of the six sectors, while preserving a mirror symmetry between the north and south halves, as well as a mirror symmetry between the east and west halves. However, in this design thin quadrupole magnets where used as a proxy for the quadrupole coefficient of the bending magnets.

After removing the artificial quadrupole magnets and adding the calculated quadrupole coefficient to the bending magnets, we ran the MAD program on the lattice file and collected the resulting optics and survey outputs. Two of the most relevant lattice parameters used in calculating the emittance are plotted in Fig. 7. The formula for emittance is then,

$$\epsilon_x = \gamma^2 C_q \frac{I_5}{I_2 - I_4} \tag{3}$$

where $C_q \approx 3.8319 \times 10^{-13}$, $\rho_x = 43.4359$[m], and

$$I_2[\mathrm{m}^{-1}] = \oint \frac{1}{{\rho_x}^2}\mathrm{ds}, \qquad I_{4x}[\mathrm{m}^{-1}] = \oint 2\frac{D_x K_1}{\rho_x}\mathrm{ds}, \quad \text{and} \quad I_{5x}[\mathrm{m}^{-1}] = \oint \frac{\mathcal{H}_x}{|\rho_x|^3}\mathrm{ds} \tag{4}$$

and $\mathcal{H}_x = \frac{D_x^2 + (\beta_x D_x' + \alpha_x D_x)^2}{\beta_x}$. By writing a small Matlab script to evaluate the integrals (4) from the optics data produced by MAD, we found the emittance to be $\epsilon_x = 3.86 \times 10^{-9}$[m].

III. FITTING TO THE WILSON RING

As the design stands, the lattice will match the Wilson ring within ±2.5m. Initially, our goal was to reduce this deviation to the order of centimeters. To approach this, we allowed individual bending magnets to vary up to 15% in strength, while still preserving the symmetry of the lattice. This variation in field strength can easily be achieved by shimming the crowns appropriately. By varying the field strength of the magnets, we allow ourselves to adjust the bend angle contributed by each magnet and thus the overall shape of the beam's path. Of course, to preserve the 360° total bend requirement, any change in the bend angle of one magnet must be balanced by an equal and opposite change to another magnet.

To begin the beam path correction procedure, we created a very simple MAD lattice file, comprised of six 60° sectors, each separated by a straight section. This lattice file represents the actual Wilson tunnel and MAD's survey data from this file was the reference path used when calculating the beam path's deviation. A Matlab script was created to take the survey output from MAD and create a list of angle and radii for both the reference and the beam path. The radii of the two paths at each respective angle were then compared and plotted as shown in Fig. 8. In order to attain a smooth function of the error, another Matlab script was created to fit an eight term Fourier series to the deviation.

Once we had the Fourier series fit of the beam path's deviation from the reference path, we attempted to correct for the deviation. A Matlab script was created to find the locations of each of the 84 bending magnets and to calculate the derivative of the Fourier series fit at each of these points. The derivative would be a measure of the discrepancy between the direction the beam path was traveling and the direction the reference path was traveling.

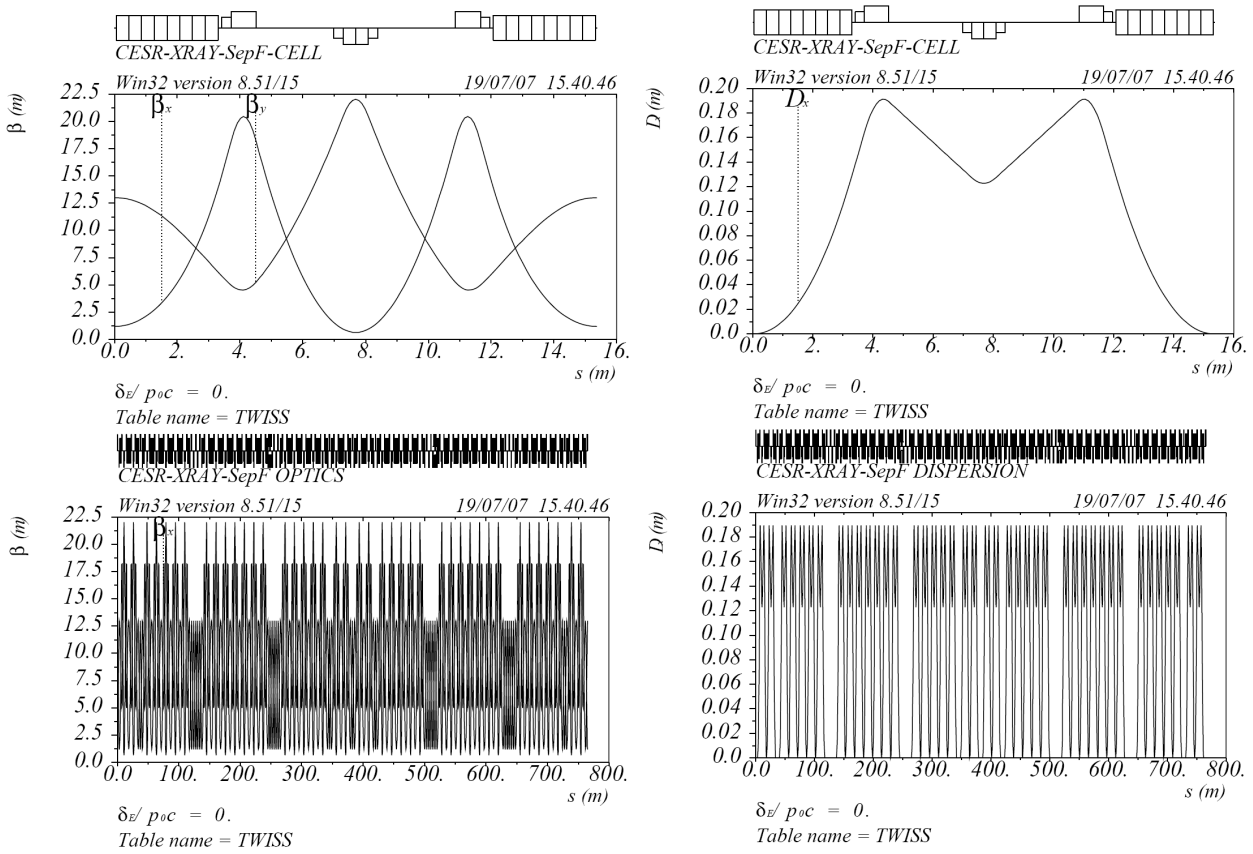

FIG. 7: The top two plots show, respectively, the β-functions and dispersion of a single cell in the lattice. The cell consists of a bending magnet, a sextupole and a quadrupole, a straight section, another sextupole and quadrupole, a quadrupole and a sextupole, a straight section, another quadrupole and sextupole, and a bending magnet. The lower two plots show, respectively, the β-functions and dispersion of the entire lattice.

Our idea was to conform the beam path by applying an "impulse" at the locations of the bending magnets in order to "kick" the beam back on course.

To apply this idea, the previous MAD lattice file was further modified to explicitly define each of the 21 unique magnetic field strengths (the remaining magnets follow by symmetry). The magnets were then given strength increases proportional to the derivatives of the deviation, at the location of each respective magnet. These strength increases were prescribed using an equation of the form, $B_{magnet_{\mathrm{X}}} = B_{magnet_{\mathrm{X}}} \times (1 + .001 \times \frac{\mathrm{d}(Deviation)}{\mathrm{d}\theta})$. The magnitude of the strength changes were purposely defined to be small, 0.1%, and the entire process was iterated, beginning with the Fourier series fitting.

Upon running this process, it was found that the initial few iteration did significantly improve the conformation of the beam path to the reference path. However, as the iterations continued, the overall deviation reached a minimum and then began to increase once again, see Fig. 9. One possible reason for the failure of this method is the fact that only the errors at the locations of the magnets were considered. Therefore, only 21 small sections of the paths were optimized and the remaining data points were not taken into account. Consequently, the major contributions to the error from this approach occurred at the locations of the straight sections between bending magnets.

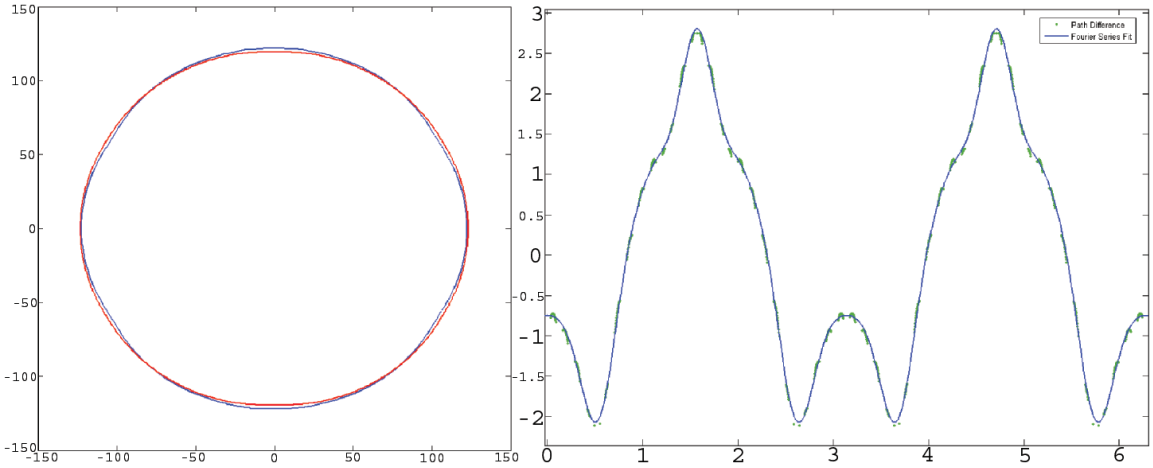

FIG. 8: The figure on the left shows a plot of the path of the proposed magnetic lattice (in red) as well as a plot of the path of the Wilson tunnel (in blue). The differences in path radii are plotted as points on the figure to the right. Superimposed on this plot is a Fourier series fit to the error. From this, we can see that the error has a span of about 5 meters.

In light of our previous oversight, our next approach to conform the beam path to the reference path involved minimizing the sum of the squared error along the entire path. For this optimization problem, we decided that a brute force approach was the simplest solution. With the brute force method, in order to obtain a solution in a reasonable amount of time, it was necessary to reconstruct some of the previously used procedures and methods. In the previous state, calling the MAD program to produce the survey output and reconstructing the data in a useable form require approximately 30 seconds per iteration. By developing a Matlab script to replicate the survey function of MAD, we were able to completely bypass the calling of MAD and reduce the previous 30 second run time to about 1 second.

In our brute force script we begin with an initial "measure of goodness" equal to the value of the sum of the squared difference between the radii of the beam path and the reference path for the entire lattice. The script begins its iterative process by randomly choosing one of the 21 unique magnets (M1) and varys the magnet by a small amount δ. Afterwards, it randomly chooses one of the remaining 20 magnets (M2) and applies the opposite change. If the measure of goodness is lower than the previous lowest measure of goodness then the values for the magnets corresponding to M1 and M2 are saved and the process is repeated. However, if the measure of goodness does not decrease with our first choice of M2, then a different M2 is chosen until either the measure of goodness decreases or until all the magnets have been tried. In either case, a new M1 is chosen and the process is repeated. This entire process is repeated until no combination of changes to M1 and M2 is found to decrease the measure of goodness, in which case δ is reduced to the value $\frac{\delta_0}{n}$, where δ_0 is the initial value for δ and n is the number of times δ has been defined. Once δ has been changed, the iterative process is again repeated. In this script, the user must define two constraints: the maximum change a magnet can undergo, in our case 15%, and the number of times δ can be decrease.

After a complete run of our brute force optimizer, we found that we could match the beam path and the reference path fairly well. With the constraint that the magnet strengths could not deviate more than 15%, we were able to reduce the original error from $\pm$2.5m to $\pm$0.5m,

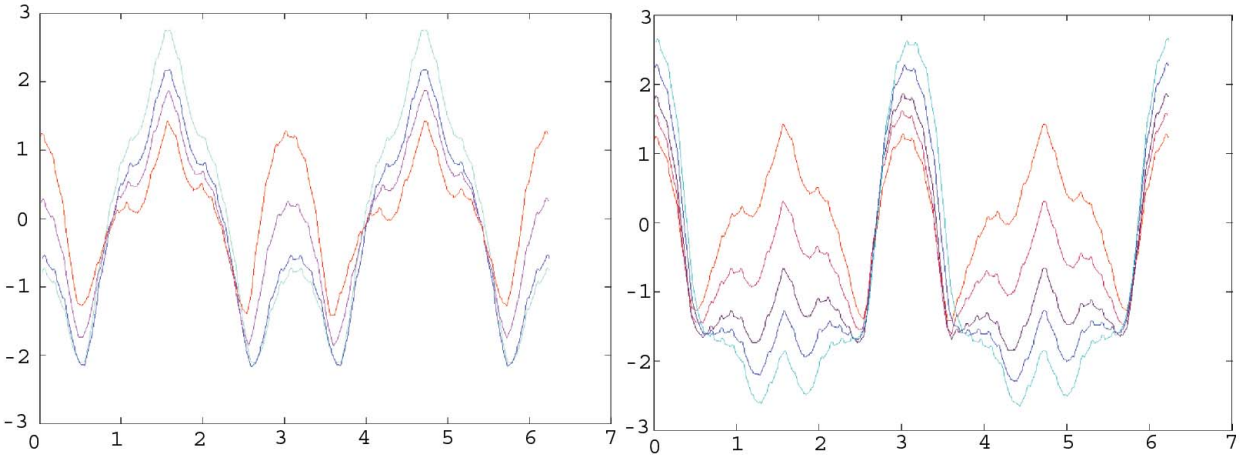

FIG. 9: These figures show superimposed plots of the difference in radii between the magnet lattice path and the Wilson tunnel. Each line is an iterations of our "direction correcting algorithm". In the plot on the left, the teal line represents the uncorrected case, the blue line represents the first iteration, the purple line represents the second iteration, and finally the red line represents the third iteration. In this plot, each subsequent iteration is an improvement on the previous one. The figure on the right is a further continuation of the iteration process, beginning at the point where the previous plot ended. The order of the iterations in color, starting from the end of the previous plot, is red, purple, navy, blue, and teal. In this plot, each subsequent iteration has a larger deviation that the previous.

see Fig. 10. Although this result does not meet our initial goal of reducing the deviations to the order of centimeters, it is adequate for purposes of fitting into the Wilson tunnel, which has a width in excess of 3 meters.

To complete the task of fitting the modified lattice to the Wilson tunnel, we once again calculate the emittance of the electron beam. Using MAD, we can minimize the emittance of the beam by applying constraints and allowing MAD to adjust the strengths of the quadrupole magnets and the distances between magnets. In this case, we define only two different quadrupoles and two different lengths and construct the magnet lattice using repetitions of these values. Here we have not rigorously attempted to minimize the emittance values exactly, but instead only attempted to preserve the β-functions, see Fig. 11 and compare with Fig. 7. The emittance value calculated from this lattice was $\epsilon_x = 3.97 \times 10^{-9}$[m], merely 3% higher than previously attained.

IV. CONCLUSIONS

The bending magnets in the existing CESR can readily be modified to be used in our proposed high brilliance x-ray source. By machining an iron crown, which can then be attached to the existing bending magnets, we can modify the magnetic field produced by the bending magnets without any additional alterations to the current magnets. This will not only make the upgrade simple and effective, but will provide for a relatively inexpensive upgrade process. As for the actual placement of the magnet lattice, we have found a configuration that conforms to the Wilson tunnel, with a small deviation of ± 0.5[m]. While this deviation is

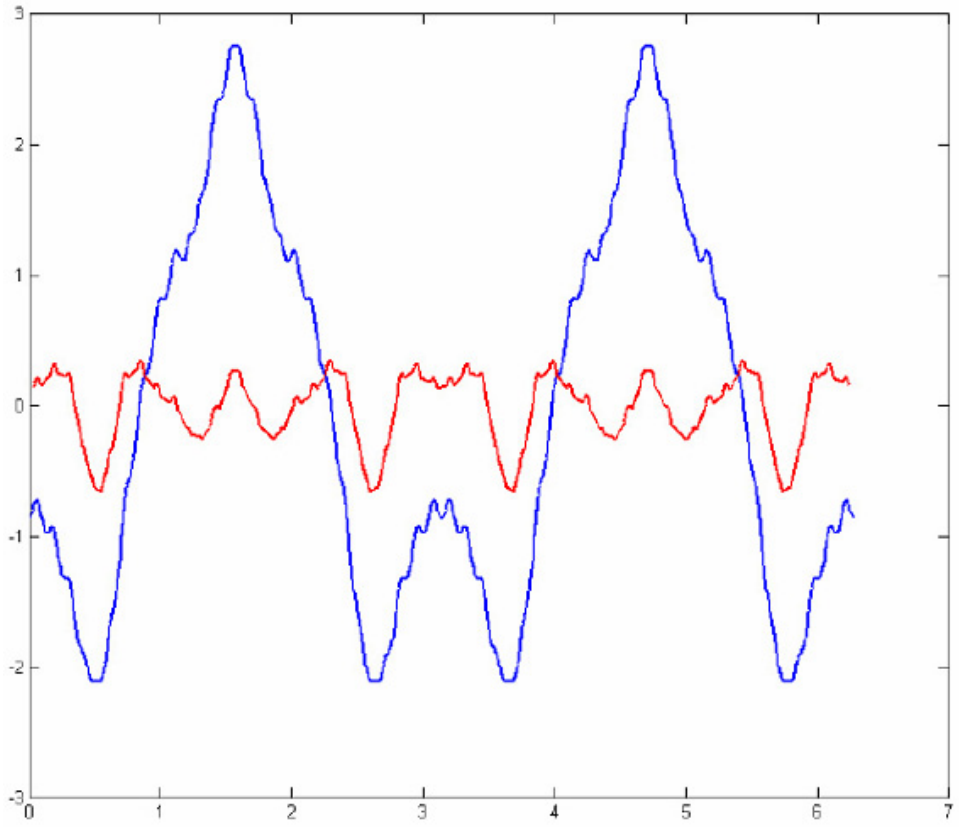

FIG. 10: A plot of the difference in radii between the magnet lattice path and the Wilson tunnel. The blue line represents the deviations before applying the brute force corrections, while the red line represents the deviations after the brute force corrections. From the plots, we can see that the brute force algorithm was able to reduce the errors from a span of 5 meters to a span of 1 meter.

certainly acceptable, one might still aspire to decrease this to the order of a few centimeters. The emittance value for this magnet lattice was found to be $\epsilon_x = 3.97 \times 10^{-9}$[m]. Again, while this value is more than adequate for the proposed plan, we can theoretically reduce this to a value of $\epsilon_x = 3.2 \times 10^{-9}$[m]. A very plausible task for the future may include improving the conformation of the beam line to the Wilson tunnel or reducing the emittance as described above. Additionally, further components of the proposed x-ray source, such as the beam transfer lines, would have to be developed and analyzed. All in all, with the creation of the bending magnet crowns and the development of the magnet lattice, we are two steps closer to having a complete detailed plan for upgrading the existing Cornell Electron Storage Ring into the brightest source of hard x-rays in the Unites States.

V. ACKNOWLEDGMENTS

First and foremost, I would like to thank my mentors Richard Talman and Ivan Bazarov of Cornell University for their discussion of ideas and their overall guidance in this research project. I would also like to thank Richard Galik and the rest of the REU staff for their time and effort in organizing this REU.

This work was supported by the National Science Foundation REU grant PHY-0552386

and research co-operative agreement PHY-0202078.

---

[1] Talman, Richard. "A Quick, Cheap, Rearranged-CESR Route to the Brilliance Frontier". Cornell University. 2007.
[2] Talman, Richard. Accelerator X-Ray Sources. WILEY-VCH, 2006.
[3] Meeker, David. Finite Element Method Magnetics. 2006.
[4] Grote, Hans, and Christoph Iselin. The MAD Program, Version 8.21.
[5] Wiedemann, Helmut. Particle Accelerator Physics I. Springer, 1999.

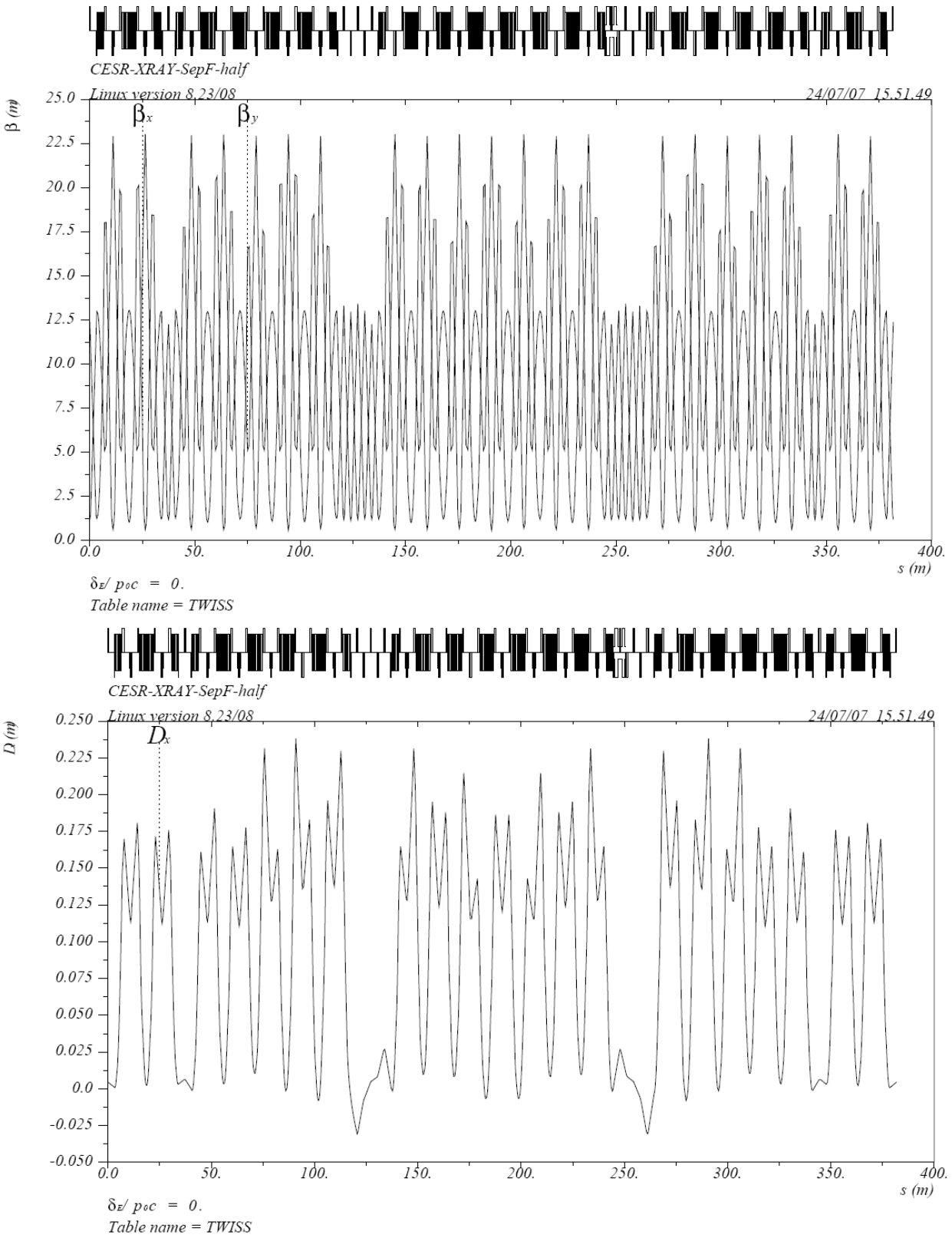

FIG. 11: These two plots show, respectively, the β-functions and dispersion of half the magnet lattice. Compared to Fig. 7 we see that the β-functions are more or less unchanged, while the dispersion has changed significantly. The resulting emittance from these β-functions and the dispersion is $\epsilon_x = 3.97 \times 10^{-9}$[m].